AGU PUBLICATIONS

Geophysical Research Letters

RESEARCH LETTER
10.1002/2015GL065409

Key Points:
- Ambient noise field used to detect unfrozen sediment thickness on arctic shelf
- Numerical modeling used to understand H/V curves observed at the seabed
- Innovative, no-impact technique for detection of permafrost in shallow water

Supporting Information:
- Text S1 and Figures S1–S5

Correspondence to:
P. P. Overduin,
paul.overduin@awi.de

Citation:
Overduin, P. P., C. Haberland, T. Ryberg, F. Kneier, T. Jacobi, M. N. Grigoriev, and M. Ohrnberger (2015), Submarine permafrost depth from ambient seismic noise, *Geophys. Res. Lett.*, *42*, 7581–7588, doi:10.1002/2015GL065409.

Received 16 JUL 2015
Accepted 3 AUG 2015
Accepted article online 6 AUG 2015
Published online 16 SEP 2015

Submarine permafrost depth from ambient seismic noise

Pier P. Overduin[1], Christian Haberland[2], Trond Ryberg[2], Fabian Kneier[1], Tim Jacobi[3], Mikhail. N. Grigoriev[4], and Matthias Ohrnberger[5]

[1]Periglacial Department, Alfred Wegener Institute Helmholtz-Center for Polar and Marine Research, Potsdam, Germany, [2]GFZ German Research Centre for Geosciences, Potsdam, Germany, [3]Institute of Earth and Environmental Sciences, University of Potsdam, Potsdam, Germany, [4]Mel'nikov Permafrost Institute, Siberian Branch-Russian Academy of Sciences, Yakutsk, Russia, [5]Institute of Earth and Environmental Sciences, University of Potsdam, Potsdam, Germany

Abstract Permafrost inundated since the last glacial maximum is degrading, potentially releasing trapped or stabilized greenhouse gases, but few observations of the depth of ice-bonded permafrost (IBP) below the seafloor exist for most of the arctic continental shelf. We use spectral ratios of the ambient vibration seismic wavefield, together with estimated shear wave velocity from the dispersion curves of surface waves, for estimating the thickness of the sediment overlying the IBP. Peaks in spectral ratios modeled for three-layered 1-D systems correspond with varying thickness of the unfrozen sediment. Seismic receivers were deployed on the seabed around Muostakh Island in the central Laptev Sea, Siberia. We derive depths of the IBP between 3.7 and 20.7 m ± 15%, increasing with distance from the shoreline. Correspondence between expected permafrost distribution, modeled response, and observational data suggests that the method is promising for the determination of the thickness of unfrozen sediment.

1. Introduction

Submarine permafrost distribution on the arctic shelves is largely untested by observation [*Stocker et al.*, 2013]. Since submarine permafrost is usually degrading relict-inundated terrestrial permafrost, modern distribution depends on rates of degradation [*Romanovskii et al.*, 2004]. Uncertainty in degradation rate translates to uncertainty on the potential impact of submarine permafrost degradation as a global climate system component [*Grosse et al.*, 2011]. On the East Siberian Shelf this applies to a region potentially as large as 1.6×10^6 km^2, the region covered by the transgression of seawater on the land following the Last Glacial Maximum. The transgression inundated terrestrial permafrost up to 100s of meters thick [*Romanovskii et al.*, 2004], creating submarine permafrost. The stability of permafrost in both settings is largely controlled by the temperature at the top of the permafrost, i.e., at the ground surface or seabed [*Lachenbruch*, 2002]. Whereas the land surface has a mean annual temperature of less than −5°C, once inundated, the seabed has a warmer temperature (> −1.8°C) [*Dmitrenko et al.*, 2011]. This leads to degradation of permafrost. This degradation is enhanced by the penetration of saline seawater into the seabed, which lowers the freezing point of the sediment's pore fluid [*Nicolsky et al.*, 2012]. The current distribution of permafrost below the seabed is thus to some degree controlled by the rate of its degradation following inundation.

Are [2003] states that "…in situ investigations of subsea permafrost dynamics are absolutely necessary…" and that "the best conditions for such investigations occur in the nearshore area of rapidly retreating coasts." Muostakh Island in the central Laptev Sea, Russia, lies within the continuous permafrost zone and has one of the longest records of rapid (up to 25 m per year) coastal erosion in the Arctic [*Günther et al.*, 2015]. Distance from the shore along these coasts thus represents a time scale, and degradation of permafrost may be observed from the time of inundation [*Are*, 2003]. Bathymetry around Muostakh Island is shallow, with seabed inclinations of 0 to 0.7% perpendicular to shore. For most investigated coastal exposures of the western and central Laptev Sea, as well as of the New Siberian Islands, Holocene deposits cover late Pleistocene Ice Complex deposits that extend down to within 10 m of modern sea level (either above or below, as at Muostakh Island). Below these silty, ice-rich deposits lie alluvial sandy silt to silty sand deposits [*Günther et al.*, 2015] up to 100s of meters in thickness [*Drachev et al.*, 1998]. Muostakh Island thus offers a variety of inundation rates within a small local setting, where sediment characteristics of the permafrost are not expected to vary greatly.

Within the sediment, the position of the boundary between unfrozen and frozen sediment depends on the temperature of the sediment, its porosity and grain size, and the concentration of the pore water solution. Methods of observation correspond to some change in bulk property between unfrozen (ice-free) and ice-bonded permafrost (IBP). Probing measures an increase in sediment hardness [*Blouin et al*., 1979], electromagnetic methods an increase in resistivity or a decrease in permittivity [*Frolov*, 1998], and seismic reflection and refraction methods an impedance contrast [*Zimmerman and King*, 1986]. Since active seismic sources may disrupt marine fauna or be relevant to resource exploration, their use is often restricted. Ambient seismic noise as source and the related analysis might form a suitable alternative in such situations. Here we use observations of the ambient noise wavefield at the seabed, particularly the spectral ratios between the average horizontal and vertical ground motion, to detect the thickness of unfrozen sediment overlying IBP.

The observation of these spectral ratios from single-station passive seismic wavefield recordings of the ambient vibration wavefield, also known as the H/V spectral ratio, has become a standard observational method in the context of shallow site assessment. Since the first works by *Nogoshi and Igarashi* [1971] in Japan, and the spread of the technique by *Nakamura* [1989] to the world, hundreds of scientific papers have been dedicated to the analysis, interpretation, and background of this cost-effective and environmentally friendly observation method.

Although it is widely accepted among authors that the microtremor H/V spectral ratio contains significant information about the near-station site structure (e.g., reviews by *Bard* [1998] and *Bonnefoy-Claudet et al*. [2006a], as well as theoretical and numerical studies by *Fäh et al*. [2001], *Bonnefoy-Claudet et al*. [2006b], *Lunedei and Albarello* [2010], and *Sanchez-Sesma et al*. [2011]), there is much debate on how to invert such data quantitatively to obtain near-surface Earth model parameters given the unknown wavefield composition in any particular case [*Fäh et al*., 2003; *Scherbaum et al*., 2003; *Arai and Tokimatsu*, 2004; *Parolai et al*., 2005; *Picozzi et al*., 2005; *Köhler et al*., 2007; *Ducellier et al*., 2013; *Hobiger et al*., 2013].

Simple 1-D-layered subsurface structures with a dominant and strong shear wave impedance contrast at shallow depth are best understood [*Malischewsky and Scherbaum*, 2004; *Bonnefoy-Claudet et al*., 2006b; *Tuan et al*., 2008; *Endrun*, 2011; *Sanchez-Sesma et al*., 2011]. For such environments—assuming an experimental setup that avoids near-field source contributions [*Chatelain et al*., 2007; *Lunedei and Albarello*, 2010]—the frequency of the fundamental peak in the H/V spectrum (lowest dominant peak frequency) can be associated with the depth of the main impedance contrast and the average shear wave velocity properties of the overlying sedimentary deposit. The peak frequency position is then a stable feature, regardless of the physical explanation for the peak origin (i.e., *SH* wave resonance, Rayleigh wave ellipticity or Airy phase of Love wave) and deviations are less than 15% for impedance contrasts larger than 3.5 [*Malischewsky and Scherbaum*, 2004; *Bonnefoy-Claudet et al*., 2008]. H/V spectral shapes on the other hand may vary significantly in appearance given the composition of the observed wavefield. The full inversion of H/V spectra has been attempted based on different prior assumptions about wavefield composition or based on estimates of surface wave dispersion from small aperture array recordings [*Fäh et al*., 2003; *Arai and Tokimatsu*, 2005; *Parolai et al*., 2005; *Picozzi et al*., 2005]. Consideration of all wavefield constituents at a single station without prior assumptions has recently been addressed by *Sanchez-Sesma et al*. [2011] in the context of diffuse wavefield theory. First steps to use their scheme for inverting velocity structures have been published recently [*Ducellier et al*., 2013; *Kawase et al*., 2011].

Our objective is to infer the thickness of the unfrozen sediment, i.e., the depth of the transition from ice-free to ice-bonded permafrost beneath the seabed ($<$20 m) around Muostakh Island. Observations of the ambient noise wavefield permit analysis of the H/V spectra peak frequency and seismic interferometry techniques are used to obtain a shear wave velocity proxy needed to calculate the thickness from the peak frequency. By cross correlation of diffuse wavefields (i.e., noise), the Green's function or seismic impulse response can be recovered, assuming that the noise sources are randomly distributed. Most of the research and application of this technique focus on the retrieval of surface waves [*Campillo and Paul*, 2003; *Shapiro et al*., 2005]. *Wapenaar* [2003], *Schuster* [2009], and *Shapiro et al*. [2005] provide overviews of the seismic interferometry technique.

2. Instrument Design and Experiment

On 8–9 August 2013, 17 submarine sensors (Figure S1 in the supporting information) were deployed around Muostakh Island in the Central Laptev Sea, Russia, along two profiles (Figure 1 and Table 1) stretching in three directions from the coastline to points about 4 km offshore of the island. Additional sensors were deployed

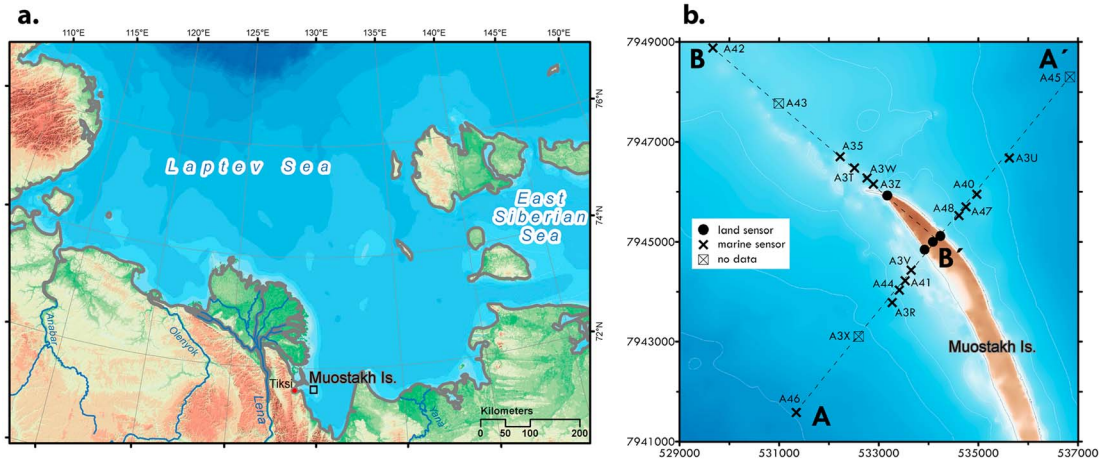

Figure 1. (a) Location of Muostakh Island in the Central Laptev Sea; (b) elevation map of the north end of Muostakh Island indicating submarine and land sensor locations along profiles A-A′ and B-B′.

on the land surface of the island, coupled to the IBP at the bottom of the seasonally thawed soil. Sensors were reacquired on 4 September 2013. The specifically designed underwater equipment consists of a low-power digital recorder continuously recording at 200 samples per second (sps), a standard short-period, three-component geophone, and a battery pack allowing for a deployment period of up to 40 days. These components are enclosed in a watertight cylindrical container safe for operation down to 100 m water depth. The recording instruments are relatively small sized and could be deployed from a small-size boat in shallow water. Details on recording equipment design are available in the supplementary online material (SOM).

3. Observations and Data Analysis

The raw data were first converted to miniseed format. The calibration signals were removed and actual sensor characteristics (eigenfrequencies and damping factors) determined. Using these values, the data

Table 1. List of Profile Station Positions and Characteristics, Including Depth to Ice-Bonded Permafrost (IBP) Calculated From H/V Frequency and From Resistivity Methods and Drilling

Profile	Station	Water Depth (m)	f_0 (Hz)	Top of Ice-Bonded Permafrost Depth (m bsf)[a]	Top of Ice-Bonded Permafrost Depth (m bsl)[a]	Permafrost Depth 2011 (m bsl) (Geolelectric Sounding)[b]	Permafrost Depth 1983 (m bsl) (Borehole Observation)[c]
B-B′	A42	3.2	2.05 ± 0.02	14.7 ± 1.8	17.9 ± 1.8	-	-
	A43	3.1	-	-	-	18.4 ± 0.7	16.2
	A3S	3	3.45 ± 0.11	8.6 ± 1.1	11.6 ± 1.1	11.0 ± 3.6	8.6
	A3T	2.2	4.15 ± 0.03	7.2 ± 0.9	9.4 ± 0.9	13.8 ± 1.6	6.6
	A3W	3.3	6.11 ± 0.06	4.9 ± 0.6	8.2 ± 0.6	8.7 ± 0.8	3.2
	A3Z	2.4	8.09 ± 0.12	3.7 ± 0.5	6.1 ± 0.5	5.4 ± 0.6	0
A-A′	A46	8.0	1.95 ± 0.06	15.5 ± 2.0	23.5 ± 2.0	-	-
	A3X	6.7	-	-	-	-	-
	A3R	5.2	1.47 ± 0.12	20.7 ± 2.6	25.9 ± 2.6	-	-
	A44	4.1	1.61 ± 0.07	18.9 ± 2.4	23.0 ± 2.4	-	-
	A41	2.6	1.51 ± 0.07	20.0 ± 2.5	22.6 ± 2.5	-	-
	A3V	2.3	2.15 ± 0.03	13.9 ± 1.7	16.2 ± 1.7	-	-
	A48	4.7	4.04 ± 0.05	7.4 ± 1.1	12.1 ± 1.1	-	-
	A47	4.9	3.31 ± 0.05	9.1 ± 1.2	14.0 ± 1.2	-	-
	A40	4.7	2.60 ± 0.03	11.5 ± 1.5	16.2 ± 1.5	-	-
	A3U	6.7	1.58 ± 0.03	19.0 ± 2.4	25.7 ± 2.4	-	-
	A45	7.8	-	-	-	-	-

[a]Calculated assuming $v = 120$ m/s.
[b]*Overduin et al.* [2015].
[c]*Slagoda* [1993].

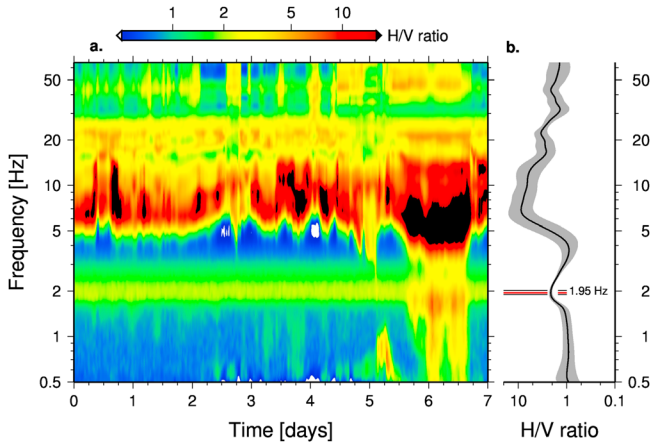

Figure 2. (a) H/V time frequency plot (one station, 1 day) for station A46 on profile A-A'; (b) stacks of the record in Figure 2a.

were restituted (see SOM). The data quality was generally good and only one marine station failed (Sensor A43, Figure 1).

In order to distinguish effects of weather (wind and rain), tides, and related currents around the island and other disturbances that may have had an influence on the recordings at the shallow sea bottom stations, we assessed the temporal variability of observations. Average H/V spectral ratios were computed on 30 min time windows following standard procedures [*SESAME*, 2004] and GEOPSY software [http://www.geopsy.org]. We used spectral estimates on 60 s time windows, with 50% overlap and spectral smoothing of horizontal (H) and vertical (V) power spectra according to *Konno and Ohmachi* [1998]. H/V ratio computation and averaging over 30 min time segments for all available data followed:

$$\frac{H}{V} = \frac{\sqrt{|H_1|^2 + |H_2|^2}}{|V|} \tag{1}$$

To check data quality, we displayed these results as time frequency plots in 24 h slices (see Figure 2). As frequency band for the analysis, we chose 0.5 Hz to 65 Hz, recognizing the low-frequency limitation of the sensors used [*Guillier et al*., 2007; *Strollo et al*., 2008a, 2008b].

We observed strong variability in H/V for most stations. Disturbances included short-lived transients that were probably related to sea surface wind wave motions and long-lasting broadband high H/V amplitude ratios probably caused by currents. The H/V ratios also showed stable features (peaks and troughs) that can be followed for hours and sometimes even days, interrupted by periods of stronger variability (Figure 2a). Periods of strong H/V amplitudes could not be correlated to weather conditions. To enhance the stable H/V parts (which we conceptually relate to the structural response of the subsurface), a manual selection of time slots was performed. The approximately 30 min segments were then stacked/averaged and variability bounds were estimated (see Figure 2b).

Lower frequencies, even below the corner frequency of the sensor, had stable long-term contributions for most of our stations, based on the means and variances. Given the good resolution capabilities of the digitizer equipment (effectively 21 bits at 200 sps), we believe that the output of the sensors at frequencies around 1 Hz can still be interpreted for most of our observations. When no clear peak could be identified, we removed the H/V estimates from those stations from further interpretation (A3X and A45, Figure 1).

At some stations we were able to observe H/V peaks at very high frequencies, some of which shifted frequency slowly with time. A large variance is associated with observations in this frequency range (Figure 2a). At low frequencies (between 1 and 10 Hz) the variance is much lower for most stations, and a flat H/V spectrum with a very small amplitude peak and neighboring trough can be observed (Figure 2b).

4. Modeling and Interpretation

The strong impedance contrast between unfrozen sediment and permafrost layer provides ideal conditions for the applicability of the H/V method. However, typical H/V applications place sensors on the free surface at the solid Earth/atmosphere boundary. In our experiment we deployed the receivers at the solid Earth/hydrosphere boundary. Previous work on the physical cause of the H/V spectral ratios does therefore not necessarily hold [*Atakan and Havskov*, 1996; *Boore and Smith*, 1999; *Bussat and Kugler*, 2011; *Frontera et al*., 2010]. To test the potential influence of the overlying water layer we performed forward modeling, calculated spectral ratios, and processed H/V data. As structural model we thus consider a three-layer model

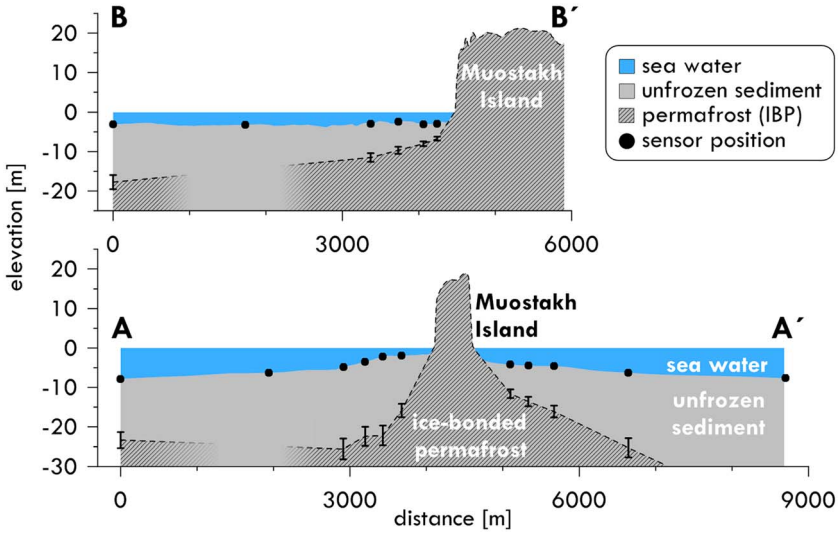

Figure 3. Cross sections of Muostakh Island and the seabed along profiles A-A′ and B-B′ (Figure 1) indicating sensor locations and the depth of the top of the ice-bonded permafrost (IBP) calculated from the H/V peak frequencies assuming a shear wave velocity of 120 m/s.

consisting of a water layer of varying depth (2 to 30 m, based on the field site bathymetry), underlain by an unconsolidated soft sediment layer with variable thickness, which was underlain by IBP that acts as a half space. For the forward computations we used the highly stable implementation of the wave number integration method by *Wang* [1999] to compute seismograms for distinct subsurface models and observation distances. We used double-couple sources of arbitrary orientation located in shallow depth in the sedimentary layer to generate complete seismograms at a number of distances (200 m to 1 km). The unfrozen, unconsolidated layer was modeled with typical elastic properties for shallow marine environments [*Stoll*, 1977].

In the modeled results, we observed a low-frequency peak in the H/V spectrum that shifts with sediment thickness (Figure S2b). It closely resembles the depth dependence of the peak frequency:

$$d = v_s/(4 \times f_0) \quad (2)$$

as expected for *S* wave resonance in an unconsolidated sedimentary layer in the two-layer case [e.g., *Malischewsky and Scherbaum*, 2004], where d is sediment thickness, v_s is the shear wave velocity of the sediment, and f_0 is the peak frequency. In addition to this low-frequency peak we observed a complex pattern of peaks and troughs at higher frequencies. For the modeled parameter range, these higher-frequency H/V peaks were clearly separated from the primary unfrozen layer signal. Varying the water layer thicknesses above the unfrozen sediment layer suggested a contribution of *P* wave resonance in the water layer (Figure S2b).

5. Results and Discussion

The low-frequency peaks, which we relate—based on the numerical modeling (see above)—to the unfrozen sediment layer between the seafloor and the IBP, varied between 1.45 and 8.08 Hz. In order to convert these frequency values to layer thicknesses, the seismic shear wave velocity of this layer is needed. We resorted to values obtained by the dispersion curve analysis of ambient noise cross correlations using all the data collected during the experiment (Figures S3 and S4). This analysis, described in the SOM, yielded an average Scholte wave group velocity of 100 m/s (±15 m/s), which corresponds roughly to layer velocities (v) of 120 ± 15 m/s for the high-frequency part of the dispersion curve associated with shallow sediments. Assuming that this value is representative for the whole study region, we estimated layer thicknesses (d) of the unfrozen sediment layer (depth of the top of the permafrost layer below the seafloor) of between 3.7 ± 0.5 m and 20.7 ± 2.6 m using equation (2) (Table 1). Strong lateral variations of the shear wave velocity in the unfrozen sediment layer would make additional measurements of sediment velocities at each measurement point necessary. The same holds for a possible depth dependence of the shear wave velocity

in the unfrozen sediment layer, since our estimates of the velocity from the dispersion curve analysis were rough and limited in resolution. However, they agree with values derived from previous experiments at the seafloor as well as from theoretical studies [e.g., *Stoll*, 1977; *Dong and Hovem*, 2011; *Vanneste et al*., 2011]. Uncertainties of peak frequencies (f_0) are obviously negligible relative to the uncertainties in the shear wave velocity. However, the modeling suggested that the $\lambda/4$ peak frequency was systematically offset from the modeled peak frequency for any given model scenario. This resembles results presented by *Malischewsky and Scherbaum* [2004] for strong shear wave contrasts. From the parameters of the modeling that we used, this offset was less than 20% in all cases. Its dependence on unfrozen sediment layer thickness and velocity is the subject of further investigation. According to equation (2), the peak frequency depends on unfrozen sediment layer thickness and average velocities. In our case, the maximum estimable depth to IBP below the seabed was around 30 m. Other conditions could require a different choice of sensor type.

The distribution of the values showed a consistent pattern and smooth spatial trends in cross sections, with lower values close to the island and higher values at greater distance from the shore (Figure 3). On Muostakh Island, IBP reaches the surface (except for the seasonally thawing layer) at the shoreline, which corresponds to 0 m thickness of the overlying unfrozen layer. The cross sections reveal the asymmetrical subsurface structure of the island, with a gentler slope off the NE shore and more abrupt deepening toward the SW. This is consistent with more rapid mean annual coastal erosion on the eastern shore (2.32 m a^{-1}) than along the western shore (0.23 m a^{-1}) between 1951 and 2012, where profile A-A′ intersects the shoreline [*Günther et al*., 2015]. To the NW the permafrost is found at shallower depth than on either side of the island. Along profile section B-B′ the depths of IBP derived by the H/V method agree to within 50 to 70 cm with the values derived in 2011 by geoelectric sounding [*Overduin et al*., 2015]. Only at station A3T was a larger difference of 4.4 m observed. The good agreement is remarkable when keeping in mind that the depth estimates were derived with different methods and without using constraining information or calibration from other methods. In boreholes drilled in 1983 along profile B-B′, the IBP was encountered at depths listed in Table 1 [*Slagoda*, 1993]. Only four borehole observations of depth to IBP are available that correspond to the determinations of the thickness of the overlying unfrozen sediment. In all cases, the observations are lower than or equal to our determinations. This is consistent with a degrading top of IBP. If all values are assumed to be correct, then mean permafrost degradation rates over the 28 year period are 13, 6, 2, and 0 cm a^{-1} in increasing distances from the shoreline (1100, 740, 410, and 230 m from shoreline in 2013), based on changes in position observed between drilling in 1983 and the 2013 measurements presented here. These values are consistent with observed submarine permafrost degradation rates near the coast (1 and 15 cm a^{-1} in less than 10 m water depth) for 12 sites with varying geomorphology and coastline change rates in the Laptev and East Siberian seas [*Overduin et al*., 2007]. The trend of decreasing mean permafrost degradation rate with increasing distance from shore is also consistent with observations of permafrost degradation following inundation [*Hutter and Straughan*, 1999]. For future applications of the H/V method for permafrost mapping, we propose calibration measurements (e.g., from boreholes or geoelectric sounding), in particular, to constrain factors affecting the velocity of the unfrozen layer.

6. Conclusions

The strong shear wave velocity contrast between the permafrost layer and the unfrozen sedimentary overburden makes the application of H/V analysis for submarine permafrost mapping very suitable. In our data set from the Muostakh Island, clear H/V peaks corresponding to the unfrozen sediment layer could be identified and confirmed by numerical modeling. We showed that the shear wave velocity of the unfrozen sediment needed to convert the H/V frequency peaks to layer thicknesses can be successfully obtained from the analysis of ambient noise cross correlations of the same data set. Therefore, the method is self-consistent and provides data without further constraints from other measurements. In our study area, the derived values of permafrost depth ($<$20 m) showed a consistent pattern with lower depth in the vicinity of the island and larger depth at greater distance to the shoreline. Where available, the derived values correlated well with those derived by electric resistivity surveys or boreholes. We estimated that the depth errors of our measurements are about 10 to 15%. Comparison with depths of the IBP from boreholes in 1983 suggests that the mean permafrost degradation rates over the 28 year period were 13, 6, 2, and 0 cm a^{-1} in increasing distances from the shoreline.

The method has a great potential for mapping the permafrost distribution in large areas with reasonable efforts. Additionally, monitoring temporal changes could be achieved by time lapse measurements. The developed low-cost, compact underwater recorders permit easy deployment from small ships and at minimal transportation costs and logistics. The method is environmentally friendly and does not need active seismic sources. Limitations of the method may include additional H/V peaks from the water layer interfering with the H/V peaks of interest. Moreover, further investigations of the velocities of the unfrozen sediment in future experiments (critical to estimate the depth of the IBP) should be conducted. Finally, the sensor frequency characteristic should correspond to the expected H/V peak frequencies depending on the permafrost depth and the shear wave velocity of the sedimentary overburden.

Acknowledgments

Data presented in this paper are available through the GIPP Experiment (GIPP Grant 201315) and Data Archive (doi:10.5880/GIPP.201315.1). Funding for the experiment was provided by a Helmholtz Association Joint Russian-German Research grant (HGF JRG-100), the Alfred Wegener Institute Helmholtz Centre for Polar and Marine Research (AWI) and by the GFZ German Research Centre for Geosciences Helmholtz Centre Potsdam. The land instruments were supplied by the Geophysical Instrument Pool Potsdam (GIPP). We thank Karl-Heinz Jäckel and Mike Hönig for their efforts in developing the underwater instruments and for sensor calibration/restitution, the GFZ Central Workshop for manufacturing the underwater casings, and WaG (Berlin) for test site provision.

The Editor thanks two anonymous reviewers for their assistance in evaluating this paper.

References

Arai, H., and K. Tokimatsu (2004), *S*-wave velocity profiling by inversion of microtremor H/V spectrum, *Bull. Seismol. Soc. Am.*, *94*(1), 53–63.

Arai, H., and K. Tokimatsu (2005), S-wave velocity profiling by joint inversion of microtremor dispersion curve and horizontal-to-vertical (H/V) spectrum, *Bull. Seismol. Soc. Am.*, *95*(5), 1766–1778.

Are, F. E. (2003), Shoreface of the Arctic seas: A natural laboratory for subsea permafrost dynamics, in *Permafrost*, edited by M. Phillips, S. Springman, and F. Arenson, pp. 27–32, Swets & Zeitlinger, Lisse.

Atakan, K., and J. Havskov (1996), Local site effects in the northern North Sea based on single-station spectral ratios of OBS recordings, *Terra Nova*, *8*(1), 22–33.

Bard, P.-Y. (1998), Microtremor measurements: A tool for site effect estimation?, in *2nd International Symposium on the Effects of Surface Geology on Seismic Motion*, vol. 3, edited by K. Irikura et al., pp. 1251–1279, A. A. Balkema, Yokohama, Japan.

Blouin, S. E., E. J. Chamberlain, P. V. Sellmann, and D. E. Garfield (1979), Determining subsea permafrost characteristics with a cone penetrometer—Prudhoe Bay, Alaska, *Cold Reg. Sci. Technol.*, *1*(1), 3–16, doi:10.1016/0165-232X(79)90014-4.

Bonnefoy-Claudet, S., F. Cotton, and P.-Y. Bard (2006a), The nature of noise wavefield and its applications for site effects studies: A literature review, *Earth Sci. Rev.*, *79*(3–4), 205–227.

Bonnefoy-Claudet, S., C. Cornou, P.-Y. Bard, F. Cotton, P. Moczo, J. Kristek, and D. Fäh (2006b), H/V ratio: A tool for site effects evaluation. Results from 1D noise simulations, *Geophys. J.*, *167*(2), 827–837.

Bonnefoy-Claudet, S., A. Köhler, C. Cornou, M. Wathelet, and P.-Y. Bard (2008), Effects of Love waves on microtremor H/V ratio, *Bull. Seismol. Soc. Am.*, *98*, 288–300.

Boore, D. M., and C. E. Smith (1999), Analysis of earthquake recordings obtained from the seafloor earthquake measurement system (SEMS) instruments deployed off the coast of southern California, *Bull. Seismol. Soc. Am.*, *89*, 260–274.

Bussat, S., and S. Kugler (2011), Offshore ambient-noise surface-wave tomography above 0.1 Hz and its applications, *Leading Edge*, *30*(5), 514–524, doi:10.1190/1.3589107.

Campillo, M., and A. Paul (2003), Long-range correlations in the diffuse seismic coda, *Science*, *299*, 547–549.

Chatelain, J.-L., B. Guillier, F. Cara, A.-M. Duval, K. Atakan, P.-Y. Bard, and the WP02 SESAME team (2007), Evaluation of the influence of experimental conditions on H/V results from ambient noise recordings, *Bull. Earthquake Eng.*, doi:10.1007/s10518-007-9040–7.

Dmitrenko, I. A., S. A. Kirillov, L. B. Tremblay, H. Kassens, O. A. Anisimov, S. A. Lavrov, S. O. Razumov, and M. N. Grigoriev (2011), Recent changes in shelf hydrography in the Siberian Arctic: Potential for subsea permafrost instability, *J. Geophys. Res.*, *116*, C10027, doi:10.1029/2011JC007218.

Dong, H., and J. M. Hovem (2011), Interface waves, in *Waves in Fluids and Solids*, edited by R. P. Vila, pp. 153–176, InTech, Rijeka, Croatia.

Drachev, S. S., L. A. Savostin, V. G. Groshev, and I. E. Bruni (1998), Structure and geology of the continental shelf of the Laptev Sea, Eastern Russian Arctic, *Tectonophysics*, *298*, 357–393, doi:10.1016/S0040-1951(98)00159-0.

Ducellier, A., H. Kawase, and S. Matsushima (2013), Validation of a new velocity structure inversion method based on horizontal-to-vertical (H/V) spectral ratios of earthquake motions in the Tohoku area, Japan, *Bull. Seismol. Soc. Am.*, *103*, 958–970.

Endrun, B. (2011), Love wave contribution to the ambient vibration H/V amplitude peak observed with array measurements, *J. Seismol.*, *15*(3), 443–472.

Fäh, D., F. Kind, and D. Giardini (2001), A theoretical investigation of average H/V ratios, *Geophys. J. Int.*, *145*, 535–549.

Fäh, D., F. Kind, and D. Giardini (2003), Inversion of local S-wave velocity structures from average H/V ratios and their use for the estimation of site-effects, *J. Seismol.*, *7*, 449–467.

Frolov, A. D. (1998), *Electric and Elastic Properties of Frozen Earth Materials*, 515 pp., Pushchino, ONTI PSC Russian Academy of Sciences (RAS), Russia.

Frontera, T., A. Ugalde, C. Olivera, J.-A. Jara, and X. Goula (2010), Seismic ambient noise characterization of a new permanent broadband ocean bottom seismometer site offshore Catalonia (Northeastern Iberian Peninsula), *Seismol. Res. Lett.*, *81*(5), 740–749, doi:10.1785/gssrl.81.5.740.

Grosse, G., V. Romanovsky, T. Jorgenson, K. W. Anthony, J. Brown, and P. P. Overduin (2011), Vulnerability and feedbacks of permafrost to climate change, *Eos Trans. AGU*, *92*(9), doi:10.1029/2011EO090001.

Guillier, B., K. Atakan, J.-L. Chatelain, J. Havskov, M. Ohrnberger, F. Cara, A.-M. Duval, S. Zacharopoulos, P. Teves-Costa, and the SESAME team (2007), Influence of instruments on H/V spectral ratios of ambient vibrations, *Bull. Earthquake Eng.*, doi:10.1007/s10518-007-9039-7.

Günther, F., P. P. Overduin, I. A. Yakshina, T. Opel, A. V. Baranskaya, and M. N. Grigoriev (2015), Observing Muostakh disappear: Permafrost thaw subsidence and erosion of a ground-ice-rich island in response to arctic summer warming and sea ice reduction, *Cryosphere*, *9*, 1–28, doi:10.5194/tc-9-1-2015.

Hobiger, M., et al. (2013), Ground structure imaging by inversions of Rayleigh wave ellipticity: Sensitivity analysis and application to European strong-motion sites, *Geophys. J. Int.*, *192*(1), 207–229.

Hutter, K., and B. Straughan (1999), Models for convection in thawing porous media in support for the subsea permafrost equations, *J. Geophys. Res.*, *104*(B12), 29,249–29,260, doi:10.1029/1999JB900288.

Kawase, H., F. J. Sanchez-Sesma, and S. Matsushima (2011), The optimal use of horizontal-to-vertical spectral ratios of earthquake motions for velocity inversions based on diffuse-field theory for plane waves, *Bull. Seismol. Soc. Am.*, *101*, 2001–2014.

Köhler, A., M. Ohrnberger, F. Scherbaum, M. Wathelet, and C. Cornou (2007), Assessing the reliability of the modified three-component spatial autocorrelation technique, *Geophys. J. Int.*, *168*(2), 779–796, doi:10.1111/j.1365-246X.2006.03253.x.

Konno, K., and T. Ohmachi (1998), Ground-motion characteristics estimated from spectral ratio between horizontal and vertical components of microtremor, *Bull. Seismol. Soc. Am.*, *88*, 228–241.

Lachenbruch, A. H. (2002), *Encyclopedia of Global Change: Environmental Change and Human Society*, edited by A. S. Goudie and D. J. Cuff, pp. 224–235, Oxford Univ. Press, Oxford, U. K.

Lunedei, E., and D. Albarello (2010), Theoretical HVSR curves from full wavefield modelling of ambient vibrations in a weakly dissipative layered Earth, *Geophys. J. Int.*, *181*(2), 1093–1108, doi:10.1111/j.1365-246X.2010.04560.x.

Malischewsky, P. G., and F. Scherbaum (2004), Love's formula and H/V-ratio (ellipticity) of Rayleigh waves, *Wave Motion*, *40*, 57–67.

Nakamura, Y. (1989), A method for dynamic characteristics estimations of subsurface using microtremors on the ground surface, *Railw. Tech. Res. Inst. Quart. Rep.*, *30*, 25–33.

Nicolsky, D. J., V. E. Romanovsky, N. N. Romanovskii, A. L. Kholodov, N. E. Shakhova, and I. P. Semiletov (2012), Modeling sub-sea permafrost in the East Siberian Arctic Shelf: The Laptev Sea region, *J. Geophys. Res.*, *117*, F03028, doi:10.1029/2012JF002358.

Nogoshi, M., and T. Igarashi (1971), On the amplitude characteristics of microtremor (Part 2) [in Japanese with English abstract], *J. Seismol. Soc. Jpn*, *24*, 26–40.

Overduin, P. P., H.-W. Hubberten, V. Rachold, N. N. Romanovskii, M. N. Grigoriev, and M. Kasymskaya (2007), The evolution and degradation of coastal and offshore permafrost in the Laptev and East Siberian Seas during the last climatic cycle, in *Coastline Changes: Interrelation of Climate and Geological Processes*, *Geol. Soc. Am. Spec. Pap.*, vol. 426, edited by J. Harff, W. W. Hay, and D. M. Tetzlaff, pp. 97–111, Geol. Soc. Am., Boulder, Colo., doi:10.1130/2007.2426(07).

Overduin, P. P., S. Wetterich, F. Günther, M. N. Grigoriev, G. Grosse, L. Schirrmeister, H.-W. Hubberten, and A. Makarov (2015), Coastal dynamics and submarine permafrost in shallow water of the central Laptev Sea, East Siberia, *Cryosphere Discuss.*, *9*, 3741–3775, doi:10.5194/tcd-9-3741-2015.

Parolai, S., M. Picozzi, S. M. Richwalski, and C. Milkereit (2005), Joint inversion of phase velocity dispersion and H/V ratio curves from seismic noise recordings using a genetic algorithm, considering higher modes, *Geophys. Res. Lett.*, *32*, L01303, doi:10.1029/2004GL021115.

Picozzi, M., S. Parolai, and S. M. Richwalski (2005), Joint inversion of H/V ratios and dispersion curves from seismic noise: Estimating the *S*-wave velocity of bedrock, *Geophys. Res. Lett.*, *32*, L11308, doi:10.1029/2005GL022878.

Romanovskii, N. N., H.-W. Hubberten, A. V. Gavrilov, V. E. Tumskoy, and A. L. Kholodov (2004), Permafrost of the east Siberian Arctic shelf and coastal lowlands, *Quat. Sci. Rev.*, *23*, 1359–1369, doi:10.1016/j.quascirev.2003.12.014.

Sanchez-Sesma, F. J., M. Rodriguez, U. Iturraran-Viveros, F. Luzon, M. Campilo, L. Margerin, A. Garcia-Jerz, M. Suarez, M. A. Santoyo, and A. Rodriguez-Castellanos (2011), A theory for microtremor H/V spectral ratio: Application for a layered medium, *Geophys. J. Int.*, *186*, 221–225.

Scherbaum, F., K.-G. Hinzen, and M. Ohrnberger (2003), Determination of shallow shear-wave velocity profiles in Cologne, Germany area using ambient vibrations, *Geophys. J. Int.*, *152*, 597–612.

Schuster, G. T. (2009), *Seismic Interferometry*, Cambridge Univ. Press, Cambridge, U. K.

SESAME (2004), Guidelines for the implementation of the H/V spectral ration technique on ambient vibrations measurements, processing and interpretation, SESAME EVG1-CT-2000- 00026, WP12, Deliverable D23.12, 62 pp.

Shapiro, N.-M., M. Campillo, L. Stehly, and M. H. Ritzwoller (2005), High-resolution surface wave tomography from ambient seismic noise, *Science*, *307*, 1615–1618.

Slagoda, E. A. (1993), Genesis i mikrostroenie kriolitogennykh otlozhenii Bykovskogo polyostrova i ostrova Muoastakh [Genesis and microstructure of cryolithogenic deposits at the Bykovsky Peninsula and the Muostakh Island] [in Russian], PhD thesis, Russian Academy of Science, Siberian Branch, Permafrost Institute Yakutsk.

Stocker, T. F., D. Qin, G.-K. Plattner, M. Tignor, S. K. Allen, J. Boschung, A. Nauels, Y. Xia, V. Bex, and P. M. Midgley (Eds.) (2013), *IPCC, 2013: Climate Change 2013: The Physical Science Basis. Contribution of Working Group I to the Fifth Assessment Report of the Intergovernmental Panel on Climate Change*, 1535 pp., Cambridge Univ. Press, Cambridge, U. K., and New York.

Stoll, R. (1977), Acoustic waves in Ocean Sediments, *Geophysics*, *42*(4), 715–725.

Strollo, A., D. Bindi, S. Parolai, and K.-H. Jäckel (2008a), On the suitability of 1 s geophone for ambient noise measurements in the 0.1–20 Hz frequency range: Experimental outcomes, *Bull. Earthquake Eng.*, *6*, 141–147.

Strollo, A., S. Parolai, K.-H. Jäckel, S. Marzorati, and D. Bindi (2008b), Suitability of short-period sensors for retrieving reliable H/V peaks for frequencies less than 1 Hz, *Bull. Seismol. Soc. Am.*, *98*(2), 671–681.

Tuan, T. T., P. G. Malischewsky, F. Scherbaum, and M. Ohrnberger (2008), Dispersion of zero-frequency Rayleigh waves in an isotropic model 'Layer over half-space', *Geophys. J. Int.*, *175*(2), 537–540, doi:10.1111/j.1365-246X.2008.03917.x.

Vanneste, M., C. Madshus, V. L. Socco, M. Maraschini, P. M. Sparrevik, H. Westerdahl, K. Duffaut, E. Skomedal, and T. I. Bjørnar (2011), On the use of the Norwegian Geotechnical Institute's prototype seabed-coupled shear wave vibrator for shallow soil characterization—I. Acquisition and processing of multimodal surface waves, *Geophys. J. Int.*, *185*, 221–236, doi:10.1111/j.1365-246X.2011.04960.x.

Wang, R. (1999), A simple orthonormalization method for stable and efficient computation of Green's functions, *Bull. Seismol. Soc. Am.*, *89*(3), 733–741.

Wapenaar, K. (2003), Synthesis of an inhomogeneous medium from its acoustic transmission response, *Geophysics*, *68*, 1756–1759.

Zimmerman, R. W., and M. S. King (1986), The effect of the extent of freezing on velocities in unconsolidated permafrost, *Geophysics*, *51*(6), 1285–1290.